Limit cycles as stationary states of an extended harmonic balance ansatz

Javier del Pino [1], Jan Košata [1], and Oded Zilberberg [2]
[1] *Institute for Theoretical Physics, ETH Zürich, 8093 Zürich, Switzerland*
[2] *Department of Physics, University of Konstanz, 78464 Konstanz, Germany*

(Received 11 August 2023; accepted 27 July 2024; published 19 August 2024)

A limit cycle is a self-sustained, periodic, isolated motion appearing in autonomous differential equations. As the period of a limit cycle is *a priori* unknown, finding it as a stationary state of a rotating ansatz is challenging. Correspondingly, its study commonly relies on numerical methodologies (e.g., brute-force time evolution, and variational shooting methods) or circumstantial evidence such as instabilities of fixed points. Alas, such approaches are (i) *unable to find all solutions*, as they rely on specific initial conditions, and (ii) do not provide analytical intuition about the physical origin of the limit cycles. Here, we (I) develop a multifrequency rotating ansatz with which we (II) find *all* limit cycles as stationary-state solutions via a semianalytical homotopy continuation. We demonstrate our approach and its performance on the Van der Pol oscillator. Moving beyond this simple example, we show that our method captures all coexisting fixed-point attractors and limit cycles in a modified nonlinear Van der Pol oscillator. Our results facilitate the systematic mapping of out-of-equilibrium phase diagrams, with implications across multiple fields of the natural sciences.

DOI: 10.1103/PhysRevResearch.6.033180

I. INTRODUCTION

Limit cycles (LCs) are periodic, isolated solutions of nonlinear differential equations that persist indefinitely in time [1]. Commonly, the oscillation period is *a priori* unknown, with oscillations reflecting the autonomous balance among the various forces acting on the system. Limit cycles are ubiquitous in all scientific fields, including physics, biology, and engineering [2,3], with broad applications, such as developing optical frequency combs and sensors [4–6], understanding biological oscillators [7–9], predator-prey community dynamics [7], chemical reaction networks [10], action potential dynamics in neural networks [11], genetics [12], designing control systems [13] and power grids [14], as well as realizing neuromorphic computing [15]. Notably, LCs have recently gained significant attention in the realm of out-of-equilibrium physics with a variety of realizations in light-matter ensembles [16–26], parametric oscillators [27–30], electromechanical systems [31–34], superconducting circuits [35], and optomechanics [36–41]. Although broadly significant, their complexity limits the ability to solve them analytically.

The precise definition of LCs varies across fields, leading to ambiguities in the literature [42,43]. We adopt the following: an LC represents self-sustained, periodic states of motion, isolated in phase space. In this state, the harmonic amplitudes that make up the LC become constant, time-invariant values, that achieve asymptotic stability for $t \to \infty$. While some definitions include complex solutions such as quasiperiodic or chaotic motions, the key feature of an LC is the absence of a preferred time origin and its resilience to phase locking to external forces. This resilience underscores LCs' key roles in synchronization [44], and fluid dynamics instabilities [45,46].

The study of LCs poses enduring challenges, due to their unknown oscillation periods and involved nonlinear dynamics. Various methods have been used for their study, including brute-force integration [47], variational shooting methods [48,49], describing-function methods [50], nonlinear functional analysis techniques [51–53], and bifurcation theory of unstable fixed points [54–56]. While useful, these methods crucially depend on an optimal choice of initial conditions (manually or through numerical single-root finding methods), or are applicable only for specific types of LCs. As such, they often fail to capture the coexistence of multiple LCs in the system. Moreover, to date, the upper bound for the number of LCs in a polynomial vector field remains unknown [57].

The Harmonic Balance Method (HBM) [58–62] is a powerful technique for finding stationary (static and periodic) solutions to ordinary differential equations (ODEs). The method employs an ansatz where the stationary solution at $t \to \infty$ takes the form of a truncated Fourier series, with series coefficients meeting analytical conditions derived from the ODEs and boundary conditions. Crucially, the complexity of determining all possible coefficient values scales exponentially with the number of degrees of freedom and coefficients [63,64], often requiring nonlinear optimization algorithms. Nonetheless, the HBM connects to the Krylov-Bogoliubov averaging method for solving nonlinear ODEs with harmonic dependence [65,66], and provides simplified analytical equations that reveal the physical mechanisms engendering LCs. Moreover and key to our work, leveraging a modern implementation of Homotopy Continuation (HC) over complex numbers [67–69], allows us to obtain all stationary

solutions semi-analytically, effectively describing various effects in nanomechanics [70–72] and light-matter systems [73–75].

In this work, we introduce a variant of the HBM that can efficiently find *all* LCs as stationary states in polynomial nonlinear ODEs. Using a truncated Fourier ansatz, and through gauge-fixing, we simplify the problem to finding the roots of a polynomial system defined by the harmonic amplitudes of LCs and system parameters. These are solved via a complex-valued HC method [67–69]. This approach offers two substantial advantages: (i) it can find complete sets of both LCs and fixed point stationary states under a generic ansatz, even when they coexist, and (ii) it facilitates semi-analytical computationally-efficient parametric studies of limit cycles, capable of detecting even isolated or unconnected LC branches. We first illustrate the merit of our approach on the prototypical Van der Pol (VdP) oscillator, which is the simplest case study for LCs. We then generalize the model to include additional nonlinearities, causing LCs and fixed point attractors to coexist. Crucially, our approach is particularly efficient for exploring the phase diagrams of nonlinear, coupled, driven-dissipative systems with many controllable parameters [28,76–78], in fields like nanomechanics, cold atoms, and nonlinear photonics. An example implementation is available within the software package HARMONICBALANCE.JL [62].

II. ILLUSTRATIVE MODEL

We consider a modified VdP oscillator that includes additional polynomial potential terms. Its displacement $x(t)$ follows Newton's equation $\ddot{x} + F(x, \dot{x}) = 0$, where

$$F(x, \dot{x}) = \omega_0^2 x + \gamma \dot{x} - \mu(1 - x^2)\dot{x} + \alpha_3 x^3 + \alpha_5 x^5, \qquad (1)$$

where the natural frequency is ω_0, γ controls the linear damping, $\mu > 0$ is the standard VdP parameter that controls the linear gain channel alongside nonlinear damping, and $\alpha_{3,5}$ are cubic and quintic nonlinearities, respectively. The limit of $\gamma = \alpha_{3,5} = 0$ in Eq. (1) recovers the standard VdP equation, where the linear gain, $-\mu\dot{x}$, drives the oscillator to higher amplitudes, and the nonlinear damping, $\mu x^2 \dot{x}$, saturates the motion into an LC (cf. the sign change of the overall term based on the value of $|x|$). Conversely, when $\mu = 0$, we have a nonlinear oscillator with quartic and sextic potential terms. The system's multiple energy minima then enable the coexistence of fixed point attractors and LCs, studied later in the manuscript.

Our model has two distinct regimes related to the sign of $(\gamma - \mu)$. A positive sign signals a damped system that will relax into one of the potential minima depending on the initial boundary conditions, see Fig. 1(a). In the opposite case (negative sign), gain overcomes damping and the system is incoherently driven to higher amplitudes, see Fig. 1(b). Generally, for each point in configuration space, $\mathbf{x}_0 = (x_0, \dot{x}_0)$, we can evaluate the Jacobian matrix $\mathcal{J}(\mathbf{x}_0)$ around that point to see where excitations flow to in the linear vicinity of $\mathbf{x}_0$. In particular, by diagonalizing the Jacobian at the origin, $\mathbf{x}_0 = (0, 0)$, we can discern between the two regimes above: the sign of the real part of the Jacobian eigenvalues $\epsilon = \frac{1}{2}(-(\gamma - \mu) \pm \sqrt{(\gamma - \mu)^2 - 4\omega_0^2})$ corresponds to whether the origin is a sink or a source (cf. discussion on the sign of $\gamma - \mu$ above); the imaginary part parametrizes the oscillation frequency for small excitations near the origin, see Fig. 1(c). These small excitations are stable and overdamped when $\gamma - \mu > 2\omega_0$, and stable and underdamped when $0 < \gamma - \mu < 2\omega_0$. The under- to over-damped transition is marked by an exceptional point [79,80]. The source-to-sink transition occurs via a supercritical Hopf bifurcation, where the excitations lose stability while maintaining their oscillation frequency. At higher gain, no notion of unstable excitations remains as the oscillation frequency is removed.

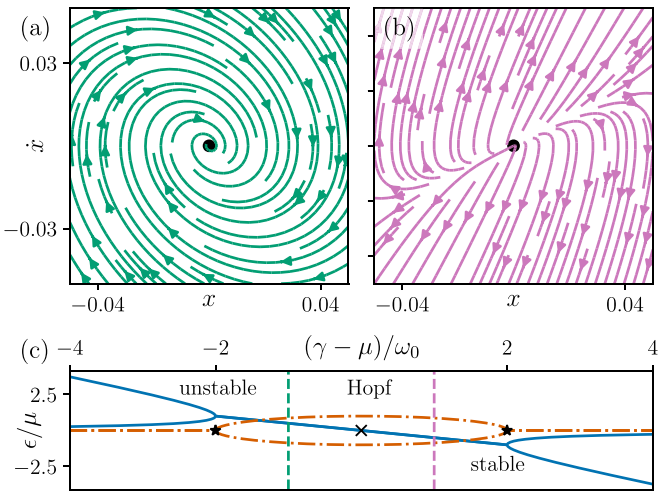

FIG. 1. Gain versus loss and Hopf bifurcations. Stream plots illustrating the behavior of a linear resonator with (a) positive loss, and (b) positive gain around the origin of parameter space (marked with black dot), cf. Eq. (1) with $\alpha_{3,5} = 0$ and $(\gamma - \mu) > 0$ or $(\gamma - \mu) < 0$, respectively. (c) A plot of the Jacobian eigenvalues around the origin (0,0) as a function of linear damping for a Van der Pol oscillator [cf. Eq. (1)]. Their imaginary part (orange, dashed-dotted lines) marks the oscillation frequency around the origin (excitation). Their real part (blue lines) denotes the inverse lifetime of the excitations (when negative) or their rate of expansion (when positive). From right to left, we observe transitions from overdamped to underdamped stable excitation (see the exceptional point at $\gamma - \mu = 2\omega_0$, star marker), to unbound (unstable) spiral (Hopf bifurcation at 0, cross marker), and to an unbound non spiraling expansion (exceptional points are at $\gamma - \mu = -2\omega_0$, star marker). Vertical dashed lines mark cases (a) and (b).

The local (sink-to-source) instability around the origin does not fully indicate whether an LC forms after a Hopf bifurcation. Indeed, without any nonlinearity in the model, the excitations will expand under the gain to infinity. However, in the standard VdP oscillator ($\alpha_{3,5} = \gamma = 0$), the nonlinear damping prevents the system from spiraling to $x, \dot{x} \to \infty$, by stabilizing an LC that encircles the origin at a distance, see Fig. 2(a). The shape of the LC changes with increasing μ, ranging from a circular orbit to a complex skewed pattern. As the LC is periodic, we can also efficiently describe it in Fourier space, see Fig. 2(b). Note that the oscillation frequency is *not* simply that of the bare resonator (ω_0). The deviation from a single harmonic circular motion is captured by the

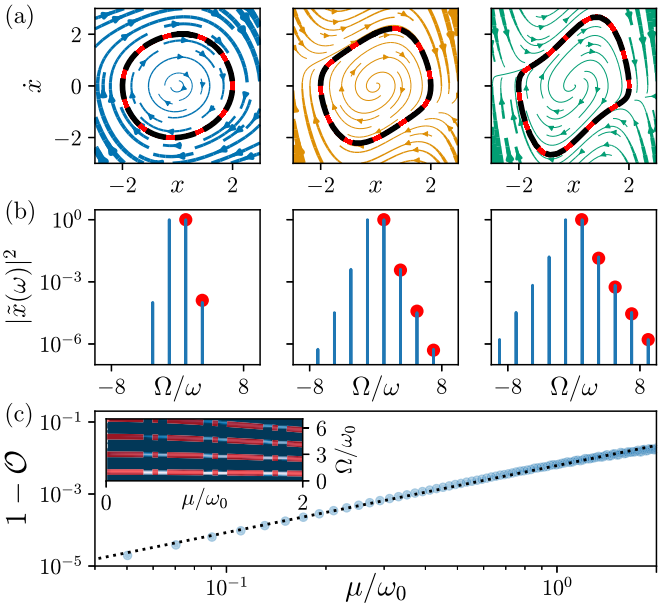

FIG. 2. The Van der Pol limit cycle and the harmonic balance method. (a) Stream plots for the VdP oscillator [cf. Eq. (1) with $\alpha_{3,5}, \gamma = 0$] show dynamics at $\mu = 0.1\omega_0$, $\mu = 0.5\omega_0$, and $\mu = \omega_0$, from left to right. The solid (red) curve marks the LC obtained from time propagation, while the dashed (black) curve represents results from the e-HBM with $M = 5$ harmonics [cf. Eq. (4)]. (b) Fourier transforms of the LC time evolutions in (a) reveal a frequency comb. Red dots show normalized squared amplitudes at odd frequencies $(2k+1)\omega\, k \in \mathbb{N}$, captured by the e-HBM. We use windowed Fourier transforms with a Hamming function to mitigate spectral leakage from finite integration times. (c) Overlap between e-HBM and exact time evolution result as a function of μ for $M = 5$. Dots show a linear fit. (inset) Same as (b) as a function of μ marking the change in the comb frequencies. e-HBM frequencies are shown as dashed lines, overlaid on the Fourier spectrum's positive frequency part.

formation of a frequency comb with Fourier amplitudes $|\tilde{x}(\omega)|^2$ at harmonics $m\omega$, $\omega \neq \omega_0$. Our LC has a half-wave symmetry in the time domain, with only odd harmonics contributing.

Due to the intricate motion of LCs, with *a priori* unknown frequencies, it is challenging to describe them as stationary states in a fixed rotating frame (frequency expansion). Instead, LCs are commonly obtained using time domain methods that involve solving a boundary value problem (BVP), cf. a detailed review in Appendix A. This requires enforcing periodicity via $x(t) = x(t+T)$, with the unknown period T determined alongside the solution. Various numerical strategies are employed to identify LCs, including direct time evolution and advanced shooting methods that transform the BVPs into initial value problems [49,81–85]. These methods are particularly effective near Hopf bifurcations [cf. Fig. 1], where LCs may emerge. Alas, these methods have limitations: (I) direct time evolution may fail to capture the LC if the initial condition is not within its basin of attraction; (II) BVPs can have multiple solutions, and the Newton-Raphson method, typically used in the final step, captures only one of them; and (III) seeding LCs out of Hopf bifurcations cannot universally capture LCs because (III-i) a sink-to-source parameter deformation of the system is required [cf. Fig. 1]; in the standard VdP with $\mu > 0$, this transition is omitted. In addition, (III-ii) LCs can arise from various types of bifurcations, and not just Hopf, e.g., from heteroclinic orbits connecting saddle points [56,66]. We overcome these limitations, in the following, by devising a variant of HBM [61] that allows us to capture LCs as stationary states of a *varying* rotating frame, i.e., at a time-evolving frequency to be discovered.

III. EXTENDED HARMONIC BALANCE METHOD

In the standard HBM ansatz, the motion

$$x(t) = \sum_{l=1}^{M} u_l(t)\cos(\omega_l t) + v_l(t)\sin(\omega_l t), \tag{2}$$

is split into M fast harmonics with frequencies $\boldsymbol{\omega} = (\omega_1, \ldots, \omega_M)$ that have slowly evolving amplitudes $\mathbf{u} = (u_1(t), \ldots, u_M(t))$ and $\mathbf{v} = (v_1(t), \ldots, v_M(t))$. The ansatz (2) approximates the time evolution with its leading frequency components. Inserting the ansatz into Eq. (1), yields (for $\alpha_{3,5} = 0$)

$$\sum_l \cos(\omega_l t)\left[\ddot{u}_l + 2\omega_l \dot{v}_l - \mu\dot{u}_l + \left(\omega_0^2 - \omega_l^2\right)u_l - \mu\omega_l v_l\right] + \sum_l \sin(\omega_l t)\left[\ddot{v}_l - 2\omega_l \dot{u}_l - \mu\dot{v}_l + \mu\omega_l u_l + \left(\omega_0^2 - \omega_l^2\right)v_l\right]$$
$$= \sum_{m,n,l} \mu[u_m \cos(\omega_m t) + v_m \sin(\omega_m t)][u_n \cos(\omega_n t) + v_n \sin(\omega_n t)] \cdot \quad [\sin(\omega_l t)(\omega_l u_l - \dot{v}_l) - \cos(\omega_l t)(\dot{u}_l + \omega_l v_l)]. \tag{3}$$

We search for stationary motion, i.e., $\ddot{\mathbf{u}} = \ddot{\mathbf{v}} = \dot{\mathbf{u}} = \dot{\mathbf{v}} = 0$. Furthermore, the premise of the HBM is to "balance" the harmonics at both sides of Eq. (3), i.e., the prefactors of each harmonic satisfy the equation independently. Nonlinear terms in Eq. (1) induce frequency mixing among different harmonics, enhanced at 'multi-photon' resonances, $\omega_l = \omega_l \pm \omega_m \pm \omega_n$. These conditions lead to the $2M$ coupled polynomial equations $\mathcal{F}(\mathbf{u}, \mathbf{v}) = 0$, containing third-degree nonlinear coupling among the prefactors of various harmonics, cf. Sec. III C. Note that finding the roots of $\mathcal{F}(\mathbf{u}, \mathbf{v})$ only solves the problem when external driving predetermines the stationary state frequencies ω_l. Further details on this standard application of the HBM can be found in Appendix B and [62].

A. Gauge fixing

Limit cycles evolve with unknown self-oscillation frequencies. We, therefore, modify the standard HBM approach and introduce a slow time variation to the frequencies, $\omega_l \mapsto \omega_l(t)$, on top of the slowly evolving amplitudes $u_l(t)$, $v_l(t)$

in the ansatz as seen in Eq. (2). In our extended HBM (e-HBM) approach, the variational prefactors evolve similarly to Eq. (3), with additional terms arising from time derivatives of $\omega_l(t)$. Now, fixing the harmonic amplitudes in the generalized stationary state, where $\ddot{\mathbf{u}} = \dot{\mathbf{u}} = \ddot{\mathbf{v}} = \dot{\mathbf{v}} = \ddot{\boldsymbol{\omega}} = \dot{\boldsymbol{\omega}} = 0$, results in a system of $2M$ coupled polynomials $\tilde{\mathcal{F}}(\mathbf{u}, \mathbf{v}, \boldsymbol{\omega}) = 0$ in the $3M$ variables $\mathbf{u}, \mathbf{v}, \boldsymbol{\omega}$. The equations are thus insufficient to determine unequivocally the LCs. Fortunately, we can deduce the missing M conditions from the spontaneous, self-oscillating nature of the LC: With no external drive to lock onto, the LC's phases are free from constraints, i.e., there is *gauge freedom* in the problem.

Gauge freedom is related to the spontaneous emergence of LCs, altering the time-translation symmetry: a time-dependent solution can appear even in a time-independent system. To illustrate this, we focus on the time translation operation by time t', such that $\mathcal{T}(t')x(t) = x(t + t')$, which is equivalent to $\mathcal{T}(\tau)a_m = a_m e^{im\omega_m\tau}$, with a complex vector $\mathbf{a} = (\mathbf{u} + i\mathbf{v})/2$. A periodic nonlinear system is invariant under the *discrete* operation $\mathcal{T}(T_s)$ with system period T_s, so it is a time-independent (autonomous) system under a *continuous*, operation $\mathcal{T}(\tau)$ with arbitrary "sampling period" τ. However, their long-term solutions can *spontaneously* break these symmetries. For instance sub-harmonic oscillations with commensurate periods $T_s q/p$ $(p, q \in \mathbb{N})$ break $\mathcal{T}(T_s)$ symmetry (harmonic generation) [30]. This allows all solutions returning to themselves after q iterations of the original translation $\mathcal{T}(T_s)$, which are related via discrete rotations $a_m \to e^{i2\pi j/q}a_m$ for $j \in \{0, 1, \ldots, q-1\}$. However, a *continuous* time-translation-symmetry-broken LC has a period that is necessarily incommensurate with any generic sampling timescale. Mathematically, the limit cycle period is τr with r irrational for a fixed τ, meaning LCs only return to their original state after infinitely many actions of $\mathcal{T}(\tau)$. This property frees oscillation phases in LCs from constraints, resulting in a continuous set of solutions, $\mathbf{a}_i$, related by full $U(1)$ symmetry $\mathbf{a} \mapsto e^{i\varphi_i}\mathbf{a}$, where $\varphi_i \in (0, 2\pi)$ [86].

The $U(1)$ gauge symmetry and the gauge-independence of the LC stationary solution allow us to fix the M gauges by redefining the time origin in Eq. (2). One possible gauge choice yields the $3M$ equations,

$$\{\mathcal{F}(\mathbf{u}, \mathbf{v}, \boldsymbol{\omega}) = 0, \mathbf{u} = 0\}. \tag{4}$$

The e-HBM equations (Eq. (4)) embody the core feedback mechanisms of LC formation (see next Sec. III C for an example). They reflect the internal balance between effective nonlinear potential, coupling and damping among harmonics, which sustains a stable orbit and *sets* its frequency (cf. Sec. III C). Our treatment simplifies when introducing relationships within $\boldsymbol{\omega}$, e.g., commensurate frequencies. For example, the LC in Fig. 2(b) exhibits a frequency comb with a single unknown frequency ω, i.e., $\omega_l = l\omega$ with $l \in \mathbb{N}$. This requires only fixing the gauge of a single harmonic to attain a solution, e.g., by setting $u_1 = 0$. Note that, our method extends beyond autonomous systems, to (non-autonomous) periodically-driven ones [17]. Here emergent harmonics in Eq. (2) become sidebands, at frequencies $\omega_d \pm \omega_l$, to the drives at ω_d.

B. Finding all solutions via a Homotopy Continuation with complex variables

Our e-HBM embeds LCs as fixed points in a high-dimensional phase space, rotating with variational frequencies ω_l. The complexity of solving the problem at this stage is delineated to the proliferation of roots in the system, which complicates the use of straightforward root-finding (e.g., Newton-Raphson) methods. Inspired by a similar challenge encountered in the standard HBM for driven motion [61], we solve Eq. (4) using HC over the complex numbers [62,64,67,68]. This method uses homotopy –a continuous deformation of an exactly solvable algebraic system into the targeted coupled polynomials– finding roots along the deformation path (Eq. (4)). Using a start polynomial system meeting or exceeding the target's root count (e.g., meeting the Bézout bound [67]) along with embedding $\mathbf{u}$, $\mathbf{v}$, ω and parameters in complex numbers ensures *all* roots are found in one run and maintains continuous root paths during deformation [68].

Applying our methodology to the VdP oscillator ($\alpha_{3,5} = \gamma = 0$), we find a single real solution that corresponds to the amplitudes $\mathbf{u}, \mathbf{v}$ and frequencies $\boldsymbol{\omega}$ that well estimate the LC [Fig. 2(a)]. This same agreement manifests more clearly in the frequency domain [see Fig. 2(b)], and persists as a function of μ for various LC frequencies, see inset of 2(c). To further validate our method, we estimate the overlap between the stationary amplitudes obtained via e-HBM and from Fourier transform of the numerical time-evolution, $\mathbf{a}_{\mathrm{FT}}$, namely $\mathcal{O} = \mathbf{a}^*_{\mathrm{HBM}} \cdot \mathbf{a}_{\mathrm{FT}}$, between the normalized harmonic amplitudes $\mathbf{a}_{\mathrm{HBM}} = (\mathbf{u} + i\mathbf{v})/\sqrt{\mathbf{u}^2 + \mathbf{v}^2}$, and $\mathbf{a}_{\mathrm{FT}}$, respectively. The overlap obeys an approximate power law $\sim(\mu/\omega_0)^2$ [cf. Fig. 2(c)] reaching few-percent deviations for $\mu = 2\omega_0$. Once a solution to Eq. (4) is found, its stability can be determined by analyzing the linear fluctuations around its vicinity, as detailed in Appendix C.

C. Convergence of the e-HBM: VdP oscillator case

The overlap's relationship with the number of harmonics in the ansatz Eq. (2), M, is not strictly monotonic due to the specific orders retained in the HBM truncation, as discussed below. We illustrate convergence challenges in the application of the e-HBM to the VdP oscillator. For the sake of simpler algebraic manipulation, we adopt a complex notation where $x(t) = \sum_{k=0}^{\frac{M-1}{2}} a_k(t)e^{-i(2k+1)\omega t} + \text{c.c.}$, where we already limited the sum to even harmonics $m = 2k + 1$, $k \in \mathbb{N}$ and c.c. denotes the complex conjugate. The first step of the HBM involves inserting such ansatz into the VdP equation Eq. (1), as illustrated in Eq. (3). Next, we match oscillatory terms with a specific frequency ω_k and isolate the corresponding frequency terms i.e. we balance the harmonics. Such frequency matching procedure filters each oscillating contribution in an equivalent way as averaging the equation over the period $2\pi/((2k + 1)\omega)$. The nonlinear damping in the VdP equation leads to couplings between different harmonic amplitudes. The corresponding term in the Harmonic Balance equation at a frequency ω_k follows from the average

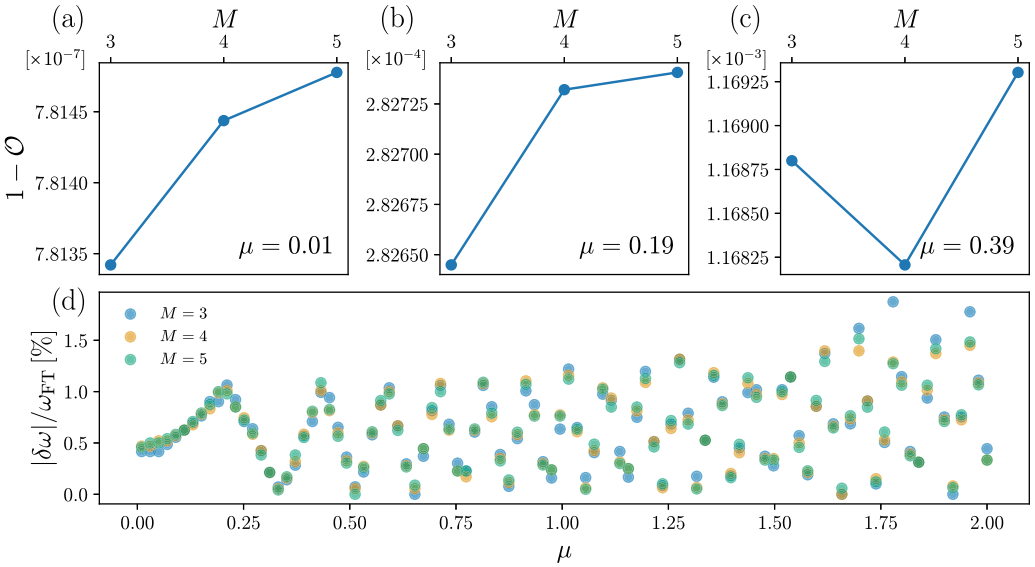

FIG. 3. Fidelity of e-HBM ansatz, further details: (a)-(c) Overlap between e-HBM and exact time evolution result as a function of the number of harmonics M for varying μ, shown at each panel [cf. Fig. 2]. The overlap is computed by matching frequency peaks in $|\tilde{x}(\omega)|^2$, from the quasi-exact evolution $\mathbf{a}_{\mathrm{FT}}$ to the nearest frequency estimates obtained by the HBM $\mathbf{a}_{\mathrm{HBM}}$, with percentual deviations below 2%, shown in (d).

integral:

$$\langle x^2\dot{x}\rangle^c = -i\frac{\omega_k}{2\pi}\int_{-\pi/\omega_k}^{\pi/\omega_k} \mathrm{d}t \sum_{m,n,p} \omega_m\left(a_m e^{-i\omega_m t} - a_m^* e^{i\omega_m t}\right) \times \left(a_n e^{-i\omega_n t} + a_n^* e^{i\omega_n t}\right)\left(a_p e^{-i\omega_p t} + a_p e^{i\omega_p t}\right)e^{-i\omega_k t}. \tag{5}$$

The equations for the harmonic amplitudes u_k and v_k can be derived by assuming $a_m(t)$ constant for the purpose of the time integration [66], and separating the real and imaginary terms from the aforementioned expression. For each k, all terms with $m, n \leqslant M$ are present, and explicitly, the surviving terms are

$$\begin{aligned}\langle x^2\dot{x}\rangle_k^c = i\sum_{m,n,p} \omega_m[a_m a_n(a_p\delta_{m+n+p+k} + a_p^*\delta_{m+n-p+k}) \\ - a_m^* a_n(a_p\delta_{-m+n+p+k} + a_p^*\delta_{-m+n-p+k})] \\ + i\sum_{m,n,p} \omega_m[a_m a_n^*(a_p\delta_{m-n+p+k} + a_p^*\delta_{m-n-p+k}) \\ - a_m^* a_n^*(a_p\delta_{-m-n+p+k} + a_p^*\delta_{-m-n-p+k})],\end{aligned} \tag{6}$$

where $\delta_{m-n} = \frac{1}{2\pi}\int_{-\pi}^{\pi} e^{i(m-n)\theta}\, d\theta$ stands for the Kronecker delta. The preceding step assumes the commensurability of frequencies, displayed by the VdP oscillator in Fig. 2(b). The ansatz insertion, expansion, and frequency balance are facilitated by the symbolic layer of the HARMONICBALANCE.JL package [62].

Equation (6) reveals explicit nonlinear coupling between different harmonics, weighted by 'selection rules' arising from the Kronecker delta factors. Some harmonics will dominate more than others in the expressions above. We observe harmonic amplitudes decaying monotonically (see Fig. 2(b)). To assess convergence, it is crucial to analyze the influence of higher-frequency harmonics on lower-frequency ones. Additionally, note that the LC in the VdP oscillator shows step functions in the time domain with half-wave symmetry and period T_s ($x(t) = -x(t \pm T_s/2)$), meaning only odd harmonics contribute to the ansatz. Therefore, the sums $\sum_{m,n,p}$ must be thus restricted to odd harmonics only, so we replace $m \to 2m+1, n \to 2n+1, p \to 2p+1, k \to 2k+1$ in the harmonic frequencies and set the origin in the indices to zero: $m, n, p, k \geqslant 0$.

Let us analyze the terms that arise from a given truncation M. Keeping only the first harmonic in the ansatz, i.e., setting $M = 1$ and collecting terms with $m = n = p = k = 0$, the only non-vanishing contributions in Eq. (6) are

$$-a_m^* a_n^* a_p \delta_{2(k-m-n+p)}, \mapsto -a_0^*|a_0|^2, \tag{7}$$

$$-a_m^* a_n a_p^* \delta_{2(k-m+n-p)} \mapsto -a_0^*|a_0|^2, \tag{8}$$

$$a_m a_n^* a_p^* \delta_{2(k+m-n-p)} \mapsto a_0^*|a_0|^2. \tag{9}$$

At this approximation level, equivalent to the lowest-order averaging method [see Ref. [66] for further details], the nonlinear dissipation in the VdP oscillator simplifies to an amplitude-dependent dispersive shift. This reduction leads to the Stuart-Landau equation [87,88], commonly used to study nonlinear oscillators near a Hopf bifurcation.

We can further analyze the corrections to this lower harmonic a_0 from the interaction between a_0 with a_1. Keeping $m, n, p \leqslant M = 1$, leads to $\langle x^2\dot{x}\rangle_{k=0}^c = -a_0^*|a_0|^2 + a_0^2 a_1^* - 2a_1 a_0^* a_1$. Similarly, keeping $m, n, p \leqslant M = 2$, introduces additional corrections,

$$\langle x^2\dot{x}\rangle_{k=0}^c = a_0^2 a_1^* - a_0\left(a_0^{*2} - 2a_1 a_2^*\right) - 2a_1 a_0^* a_1^* - a_2 \times \left(a_1^{*2} + 2a_0^* a_2^*\right), \tag{10}$$

where a_0 and a_2 are directly coupled, but also a_0, where a_0, a_1, and a_2 have a threefold interaction. At increasing orders,

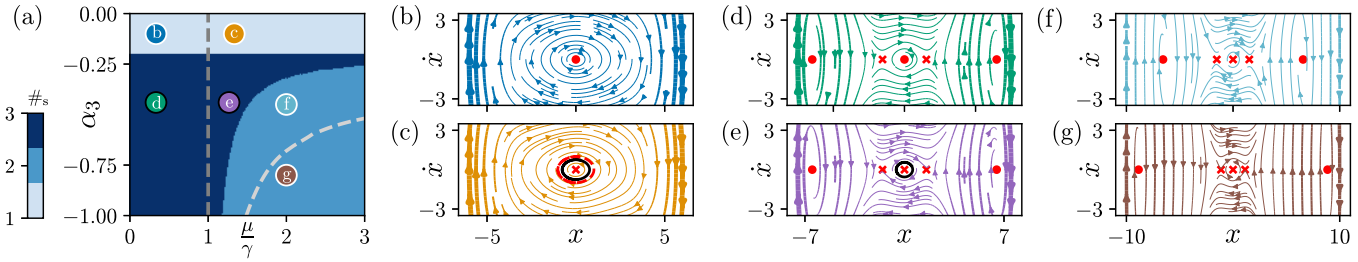

FIG. 4. Coexistence of limit cycles and fixed points. (a) Phase diagram of the model (1) in the α_3, μ parameter space, showing the count of stable stationary states, $\#_s$, including LCs and fixed points. Dashed lines mark boundaries where the number of unstable stationary states changes. Panels (b)-(g) illustrate distinct flow patterns in each region [cf. Fig. 1]. Stable (unstable) HBM fixed points are depicted by dots (crosses). The LC found by the e-HBM is shown by a red dashed line. Regions (b) and (d) exist below the Hopf bifurcation, i.e., $\mu < \gamma$, and only sustain fixed points. When $\mu > \gamma$, regions (c) and (e) host an LC around the origin, that coexists with stable fixed points in (e). The transition between (b) and (d) [respectively (c) and (e)] is associated with the appearance of two additional fixed points. The LC destabilizes in (f) and vanishes in (g) by merging with the unstable fixed points, and leaves behind solely fixed points. In all panels, $\omega_0 = 1$, $\mu = 0.1$, $\gamma = 0.03$, $\alpha_5 = -0.01$, and $M = 2$.

nonlinear contributions between all harmonics proliferate, see

$$\begin{aligned}\langle x^2\dot{x}\rangle^c_{k=0} = {} & a_0^2 a_1^* + a_0\big[2(a_1 a_2^* + a_2 a_3^* + a_3 a_4^*) - a_0^{*2}\big] \\ & - a_2 a_1^{*2} - a_4 a_2^{*2} - 2a_2 a_0^* a_2^* - 2a_3 a_1^* a_2^* + a_1^2 a_3^* \\ & - 2a_3^*(a_3 a_0^* + a_4 a_1^*) + a_1(2a_2 a_4^* - 2a_0^* a_1^*). \quad (11)\end{aligned}$$

The Fourier analysis [cf. Fig. 2(b)] indicates that $a_k \mapsto 0$ as k increases, suggesting that the terms $a_m a_n a_p$ become progressively weaker with higher harmonics, leading to expected convergence. However, further analysis is required to determine if this convergence is monotonic. As shown in Fig. 3, increasing the number of harmonics M in the ansatz does not necessarily enhance the solution's fidelity. Further research into the convergence of multiharmonic and higher-order Krylov-Bogoliubov methods is delegated to future work.

IV. COEXISTENCE OF A LIMIT CYCLE WITH FIXED POINTS

The combination of our e-HBM and the complex-valued HC simultaneously captures all solutions, outperforming time-evolution or shooting methods that explore one solution per run [49]. It also improves upon traditional HBMs that use single-variable real continuation [46,89]. When $\alpha_{3,5} = 0$, the system sustains a unique LC around the origin, as guaranteed by Lienard's theorem [90], but with $\alpha_{3,5} \neq 0$ various stationary states coexist, see Fig. 4(a), due to the conservative potential that hosts multiple energy minima. To describe this coexistence using e-HBM, we apply a two-step procedure: (i) we first solve for stationary fixed-points using a zero-frequency ansatz $x(t) = a_0(t)$, and then (ii) find LCs using the e-HBM ansatz (Eq. (2)). This approach requires an ansatz that includes a zero-frequency harmonic alongside harmonics with $(2l+1)\omega$ frequencies, where $l \in \mathbb{N}$. Notably, the HBM and the e-HBM are mutually exclusive: HBM captures only the trivial fixed point for a_0 in the VdP oscillator (the origin), but misses LCs, while the e-HBM's gauge fixing fails at time-independent fixed points, resulting in infinitely-degenerate solutions of zero amplitude around fixed points, due to the arbitrariness of $\boldsymbol{\omega} \neq 0$. Luckily, by combining the results from the two steps, we fully capture the stationary solutions of the system (including LCs) for different parameters, e.g., as a function of the cubic potential and nonlinear gain, and obtain the phase diagram of the system, see Fig. 4(a). We observe distinct regions, including a stable LC that coexists with fixed point attractors at region, see Fig. 4(e). This coexistence exemplifies the loose connection between Hopf bifurcations and LCs, as no bifurcation appears, see, e.g., transition between regions in Figs. 4(e) and 4(f). In this work, we explore the parameter regime where LCs coexist with fixed points, without delving into potential intersections between them. As μ increases, LCs can merge with saddle points and become only semi-stable. Crucially, the coexistence of LCs and fixed points applies to phenomena like the heart's rhythmic beating and oscillating chemical reactions [2,44], highlighting the broad applicability of the approach.

V. CONCLUSION AND OUTLOOK

Our method, available through HarmonicBalance.jl package [62], facilitates the investigation of LCs in a breadth of fields. Instead of relying on numerical evolution and single-root finding, our e-HBM approach employs a complex-valued HC method to identify LCs as fixed points within a rotating ansatz. Our treatment can be readily extended to nonautonomous systems with periodic forcing, whose dynamics spontaneously shifts from periodic to quasiperiodic behavior [27]. It allows us to uncover multiple coexisting LCs and stable phases, and in particular multiple LCs within the same system [91,92]. This makes our approach well-suited for the analysis of many-body phases in mean-field problems [93–95], frequency combs [96], and synchronization conditions or parametric symmetry breaking in classical and quantum oscillator arrays [21,97–108]. Notably, in all these fields, the ability to describe the LCs as a fixed point provides the framework for studying stochastic dynamics and activation between LCs. Last, the effectiveness of our e-HBM hinges on efficiently solving $2M$ coupled polynomial equations [109]. Progress towards efficiently solving the Eq. (4) will allow us to solve complex systems with more degrees of freedom [63].

ACKNOWLEDGMENTS

We thank A. Eichler, A. Nunnenkamp, and C.W. Wächtler for fruitful discussions. J.d.P. was supported by the ETH Fellowship program (Grant No. 20-2 FEL-66). J.K. was supported by the Swiss National Science Foundation through Grant No. CRSII5 177198/1. O.Z. acknowledges funding through SNSF Grant No. CRSII5_206008/1, and the Deutsche Forschungsgemeinschaft (DFG) through Project No. 449653034, and via SFB1432.

APPENDIX A: FINDING LIMIT CYCLES: SUMMARY OF NUMERICAL METHODS

Here we aim to provide a comprehensive overview of the various numerical methodologies used for calculating limit cycles in nonlinear dynamics. Although we endeavor to cover a broad spectrum of techniques, we encourage interested readers to consult [110,111] for a more extensive exploration of the topic.

Without loss of generality, we consider an LC to be a periodic solution $\varphi(\mathbf{x}_0, t)$, propagated from the initial condition $\mathbf{x}_0 \in \mathbb{R}^n$ for a time t, of the autonomous system

$$\dot{\mathbf{x}} = f(\mathbf{x}), \tag{A1}$$

i.e., such that

$$\varphi(\mathbf{x}_0, T) - \mathbf{x}_0 = 0. \tag{A2}$$

Remarkably, Eq. (A2) indicates that finding LCs involves solving a two-point boundary value problem (BVP), which is typically more complex than an initial value problem (IVP). Numerical methods address the BVP usually by merging time evolution from an IVP with the optimization of initial conditions and the frequency or period of the limit cycle. The optimization problem involved is nonlinear, and iterative root-finding techniques like the standard Newton-Raphson method are employed to solve it. Note that, due to the reliance of IVPs on the initial condition $\mathbf{x}_0$, the following algorithms are designed to capture only a single LC per execution.

1. Single shooting method

This approach transforms the BVP equations (Eqs. (A1) and (A2)) into an IVP, iteratively adjusting initial conditions to identify a closed orbit. The basic form of the shooting method, known as single shooting, involves the following steps until convergence: (i) *aiming*, or initially guessing $\mathbf{x}_0$, usually based on prior knowledge about the LC, followed by (ii) *shooting*, i.e., integrating numerically (A1) from $\mathbf{x}_0$ to find $\varphi(\mathbf{x}_0, T_s)$. This integration should span a time interval approximately equal to the anticipated (but unknown) period of the LC. The final steps involve (iii) *assessing condition (A2)*, i.e., evaluating the trajectory's endpoint to ascertain whether the trajectory returns to its starting point, and finally (iv) *readjusting* the initial conditions based on the trajectory's failure to form a closed loop. This entails solving the nonlinear system $\varphi(\mathbf{x}_0, T_s) - \mathbf{x}_0 = 0$ for the initial condition $\mathbf{x}_0$ and the period T_s by applying iterative root-finding methods (e.g., Newton-Raphson). Step (iv) is typically supplemented by an additional constraint of the form $s(\mathbf{x}_0, T_s) = 0$, which includes a phase condition akin to the gauge fixing of the e-HBM ansatz in the main text, in order to remove redundancy of solutions under continuous time translations. Note that the *Multiple shooting method* modifies this approach by breaking the solution into smaller time segments. For each segment, an initial value problem is solved, and the solution is refined similarly to the single shooting method, but with additional matching conditions to stitch these segments into a complete solution spanning the entire interval.

2. Poincaré shooting

This is a variant of the shooting method that exploits the concept of a Poincaré section [2]. A Poincaré section is a lower-dimensional surface intersecting the phase space of the dynamical system (e.g., a line in two dimensions). (i) *Aiming:* In this method, a Poincaré section is chosen so that a periodic orbit, if it exists, will intersect it at some point. (ii) *Shooting* then takes place from an initial guess on the Poincaré section. (iii) The trajectory of the system is monitored until it intersects the Poincaré section again. This might happen after one or more cycles of the underlying dynamics. (iv) The difference between the initial point and the point where the trajectory intersects the Poincaré section again (after completing a loop) is calculated. The last step involves (v) iterative refinement of the initial condition *within* the Poincaré section (e.g., through root-finding algorithms). Note that finding periodic orbits means identifying the fixed points on the Poincaré map: This map tracks where trajectories cross the Poincaré section. Periodic orbits cross this section at the same point every period. A significant limitation of this algorithm is its dependency on pre-existing knowledge of the LC's location. For more information on constructing the algorithm on the Poincaré section, see Ref. [112].

3. Trapezoidal method

This method addresses the BVP by segmenting the time evolution into slices and applying the trapezoidal rule for finite differences – similar to a Runge-Kutta method for solving ODEs– to compute the evolution over each slice for $\mathbf{x}_0$ and T_s, while adhering to the constraint $\mathbf{x}(0) = \mathbf{x}(T_s) \equiv \varphi(\mathbf{x}_0)$. Because T_s is unknown beforehand, we commonly solve a system equivalent to Eq. (A1) over a fixed interval [0,1] by rescaling time.

$$\dot{\mathbf{x}} = T_s f(\mathbf{x}), \quad \mathbf{x}(0) = \mathbf{x}(1). \tag{A3}$$

A supplementary phase condition, akin to both shooting method and e-HBM is added to remove redundancy in solutions due to continuous time translations. The following integral constraint is typically used:

$$\int_0^1 ds \;\; \mathbf{x}(s) \cdot \dot{\mathbf{x}}_{\text{old}}(s) = 0, \tag{A4}$$

where $\dot{\mathbf{x}}_{\text{old}}(t)$ is the tangent vector of a previously calculated LC and is therefore known. The finite difference system, for which we seek a solution, takes the following form according to the trapezoidal rule:

$$\mathbf{x}_j - \mathbf{x}_{j-1} - \frac{T_s}{2}(f(\mathbf{x}_j) + f(\mathbf{x}_{j-1})) = 0, \tag{A5}$$

with $\mathbf{x}_m - \mathbf{x}_1 = 0$, for $j = 1, \cdots, m-1$. The system's solution is derived by solving Eq. (A5) and condition (A3), typically using iterative (e.g., Newton) solvers.

4. Orthogonal collocation

In this case, the rescaled time interval [0,1] in Eq. (A3) is first divided into R smaller "test" intervals $0 = \tau_0 < \tau_1 < \cdots < \tau_R = 1$, on each of which the solution $\mathbf{x}(\tau)$ is approximated by an order m vector valued polynomials $\mathbf{x}^{(i)}(\tau)$. This is done by defining $m+1$ equidistant mesh points on each test interval:

$$\tau = \tau^{(j)}(\sigma) \equiv \tau_j + \frac{(1+\sigma)}{2}(\tau_{j+1} - \tau_j), \tag{A6}$$

with $\sigma \in [-1, 1]$. The functions $\mathbf{x}^{(j)}$ defined on $[-1, 1]$ by $\mathbf{x}^{(j)}(\sigma) \equiv \mathbf{x}(\tau_j(\sigma))$ satisfy

$$\dot{\mathbf{x}}^{(j)} = T_s \frac{\tau_{j+1} - \tau_j}{2} \cdot f(\mathbf{x}^{(j)}), \tag{A7}$$

with the continuity equation on $[-1, 1]$, $\mathbf{x}^{(j+1)}(-1) = \mathbf{x}^{(j)}(1)$. The equations are solved using a polynomial approximation of degree m, achieved by setting a partition $-1 = \sigma_1 < \cdots < \sigma_i < \cdots < \sigma_{m+1} = 1$ to establish *collocation* points $\tau_{i,j} = \tau^{(i)}(\sigma_j)$. The associated $m+1$ lowest degree interpolating (Lagrange) polynomials of degree m, with collocation points as roots, are

$$\mathcal{L}_i(\sigma) \equiv \prod_{k=1, k\neq i}^{m+1} \frac{\sigma - \sigma_k}{\sigma_i - \sigma_k}, \tag{A8}$$

for $i = 1, \ldots, m+1$. The approximation for $\mathbf{x}(\tau)$ reads $p_j(\sigma) \equiv \sum_{k=1}^{m+1} \mathcal{L}_k(\sigma) x_{j,k}$, where $x_{j,k}$ denotes the k-th component of $\mathbf{x}^{(j)}$. The optimal collocation method, employs Gaussian quadrature for efficient numerical integration of the equation. This is accomplished by matching collocation points the nodes z_l in the Gauss–Legendre quadrature rule. The problem to solve reduces then to

$$\dot{p}_j(z_l) = T \frac{\tau_{j+1} - \tau_j}{2} f(p_j(z_l)), \tag{A9}$$

with $1 \leqslant l \leqslant m, \quad 1 \leqslant j \leqslant R$. Besides the unknown period T_s, solving for $x_{j,k}$ involves $nR(m+1)$ unknowns for a vector $\mathbf{x} \in \mathbb{R}^n$. Similarly to previous methods, to ensure the uniqueness of solution, it is necessary to incorporate the phase condition represented by the integral $1/T_s \int_0^{T_s} \mathrm{d}s \;\; \mathbf{x}(s) \cdot \dot{\mathbf{x}}(s) = 0$.

5. Available software

The methods we reviewed are designed to identify one LC at a time, typically near a known Hopf bifurcation. After discovering an LC, its parametric dependence can be traced using numerical continuation methods. Such methods are featured in established software suites including AUTO/XPPAUT [81,82], MATCONT [84], PYDSTOOL/PYCONT [113], CoCo [85], and BifurcationKit [49]. These tools generally employ pseudo-arclength continuation on real parameters [48]. However, such methods are typically restricted to finding and tracking a single solution path per computational thread, potentially missing isolated solution branches. In contrast, our Homotopy Continuation method utilizes a complex embedding approach, enabling the identification of *all* complex roots to the Harmonic Balance equations, therefore all physical, real solutions [63,68]. This method also allows for the continuation towards *every* real solution for all parameters, effectively managing multiple solution paths over complex variables simultaneously. Note that the effectiveness of the homotopy continuation method we use is largely due to its application to a particular kind of nonlinear problem, i.e., to problems that effectively map to root finding of a set of polynomial equations that have a positive degree. This method operates by simplifying nonlinear terms into polynomial forms or transforming specific equation types, such as trigonometric ones, into polynomials using appropriate transformations. Our implementation of this method is fully documented and publicly accessible through HARMONICBALANCE.JL package [62,114].

APPENDIX B: HARMONIC BALANCE METHOD

The Harmonic Balance Method (HBM) is commonly applied to handle harmonically driven nonlinear systems. Such systems are described by general nonlinear system of N second-order ODEs of the form

$$\dot{\mathbf{x}}(t) = \mathbf{G}(\mathbf{x}(t), t), \tag{B1}$$

where $\mathbf{x}(t) = (x_1(t), x_2(t), \cdots, x_N(t))^T$, and $x_i(t)$ are real variables with $i = 1, 2, ..., N$ and time t as the independent variable. The function $\mathbf{G}(\mathbf{x}(t), t)$ is assumed to depend harmonically on $\mathbf{x}(t)$ and its time derivatives. Note that in a linear system, $\mathbf{G}(\mathbf{x}, t) = \ddot{\mathbf{x}} + \mathbf{M}\mathbf{x} + \mathbf{b}(t)$, where $\mathbf{M}(t)$ contains spring constants and linear couplings, and $\mathbf{b}(t)$ represents external forces. Diagonalizing $\mathbf{M}$ yields the normal modes of the system.

The system (B1) eventually reaches a stationary state, typically showing an oscillatory response with a constant amplitude over time. The HBM assumes such solutions can be represented by the expansion

$$x_i(t) = \sum_{l=1}^{M_i} u_{l,i}(t) \cos(\omega_{l,i} t) + v_{l,i}(t) \sin(\omega_{l,i} t), \tag{B2}$$

where we introduced M_i harmonics oscillating at frequencies $\omega_{l,i}$ with slowly-varying envelopes $u_{l,i}(t)$ and $v_{l,i}(t)$, in order to describe the evolution of each variable $x_i(t)$. An approach to finding such amplitudes involves using ODE solvers to propagate the evolution over a long time and then performing Fourier analysis on the solutions. Once a given set of solutions has been found for a parameter set, additional solutions can be obtained by continuation techniques [61]. This methodology, however, can be challenging to apply, since nonlinear systems can have multiple stationary states, resulting in different responses depending solely on the initial conditions. Time-consuming initial condition sampling is needed to map all stationary-state branches, but it may not reveal every solution branch.

To simplify the process, an alternative approach involves using Eq. (B2) as an ansatz of the ODE system. Replacement of the expansion of Eq. (B2) into Eq. (B1) leads to harmonic oscillating terms at both sides of the equation. The

stationary state problem can be transformed into an algebraic one, within the truncated ansatz Eq. (B2), by balancing harmonics at both sides of Eq. (B1). This procedure results in equations equivalent to those found by Krylov-Bogoliubov averaging [62,66]:

$$\mathcal{F}(\mathbf{u}, \mathbf{v}) = 0, \tag{B3}$$

where $\mathbf{u} = (u_{1,1}, \cdots, u_{M_N,N})$, $\mathbf{v} = (v_{1,1} \cdots, v_{M_N,N})$.

In typical scenarios, an externally driven system settles into stationary motion states that oscillate at frequencies that are equal or commensurate with the driving frequencies. Therefore, the frequencies $\omega_{l,i}$ can be assumed *a priori* (e.g., they are prescribed by the driving frequencies), while the variables $\mathbf{u}$, $\mathbf{v}$ remain unknown. The resulting algebraic conditions Eq. (B3) can be solved using the homotopy continuation method. In short, this method starts with an analytically-solvable polynomial of the same order, deforming it into the target polynomial and tracking the roots. For example, to find the roots of a p-th order polynomial $\mathcal{P}(z)$, one starts with $\mathcal{U}(z) = z^p - 1$, which has known roots $\mathbf{q}_0$. A generalized approach tracks such roots to those of $\mathcal{F}$, denoted $\mathbf{u}_0$, leading to an exponential number of solution paths. To manage this, a two-step *parameter homotopy* algorithm reduces computational overhead (see [114]). Note that only real roots are physically meaningful.

APPENDIX C: STABILITY ANALYSIS

Assume we found a real solution $\mathbf{u}_0$ of Eq. (B3). The system's response to small perturbations determines its stability. To analyze this, we linearize Eq. (B1) ar ound $\mathbf{u}_0$ with a small perturbation $\delta\mathbf{u} = \mathbf{u} - \mathbf{u}_0$:

$$\frac{d}{dT}[\delta\mathbf{u}(T)] = J(\mathbf{u}_0)\delta\mathbf{u}(T), \tag{C1}$$

where $J(\mathbf{u}_0) = \nabla_{\mathbf{u}}\mathcal{F}|_{\mathbf{u}_0}$ is the Jacobian matrix. The solution to Eq. (C1) is

$$\delta\mathbf{u}(T) = \sum_{r=1}^{2NM} (\mathbf{e}_r \cdot \delta\mathbf{u}(T_0))\mathbf{e}_r e^{\lambda_r T}, \tag{C2}$$

where λ_r and $\mathbf{e}_r$ are the eigenvalues and eigenvectors of $J(\mathbf{u}_0)$. Here, T represents a "coarse-grained" timescale that is much slower than the oscillations in the system ($T \gg 2\pi / \min\{\omega_{l,i}\}$ in Eq. (B2)) [62,66]. If $\mathrm{Re}(\lambda_r) < 0$ for all r, $\mathbf{u}_0$ is stable. If $\mathrm{Re}(\lambda_r) > 0$ for any r, it is unstable. The workflow involving the ansatz Eq. (B2), its insertion into the system Eq. (B1), finding the real roots of the resulting algebraic conditions Eq. (B3), and analyzing the stability of solutions is fully automated in the HARMONICBALANCE.JL software suite [62].

For LC analysis, stability analysis proceeds similarly, but with additional numerical consideratio ns:

(i) Solutions with $\boldsymbol{\omega} = 0$ are labeled unphysical—in addition to those with non-real $\mathbf{u}, \mathbf{v}$ coefficients—as they contradict the assumption of distinct harmonic variables.

(ii) The Jacobian in Eq. (C1) is found as in the standard HBM. With a $U(1)$ gauge freedom, an infinite set of neighboring steady states exists, meaning perturbing the free phase leads to a new steady state rather than returning to or diverging from the original. This manifests in an eigenvalue $\lambda_r = 0$. To resolve this, stability can be redefined as $\mathrm{Re}(\lambda_r) \leqslant 0$ or resolved by gauge fixing the Jacobian. This makes the matrix singular, which can be handled by noting the promotion of the unknown LC frequencies $\boldsymbol{\omega}$ to a variable.

(iii) After gauge fixing, solutions still show a four-fold degeneracy due to: (i) a double degeneracy from the arbitrary sign of the frequency $\boldsymbol{\omega}$ in the ansatz, and (ii) another double degeneracy from two phase choices compatible with a given gauge choice, e.g., $u_1 = 0$ can be achieved by both $\phi = \pi/2$ and $\phi = 3\pi/2$ in a rotation of the form $\mathbf{a} \mapsto \mathbf{a}e^{i\phi} = \mp\boldsymbol{v}$.

[1] C. Christopher and C. Li, *Limit Cycles of Differential Equations*, Advanced Courses in Mathematics - CRM Barcelona (Birkhäuser Basel, 2007).

[2] S. H. Strogatz, *Nonlinear Dynamics and Chaos: With Applications to Physics, Biology, Chemistry and Engineering* (Westview Press, Boca Raton, FL, 2000).

[3] L. Edelstein-Keshet, 8. Limit cycles, oscillations, and excitable systems, in *Mathematical Models in Biology* (Society for Industrial and Applied Mathematics, Philadelphia, USA, 2005), pp. 311–380.

[4] S. Kim, Y. G. Rubo, T. C. H. Liew, S. Brodbeck, C. Schneider, S. Höfling, and H. Deng, Emergence of microfrequency comb via limit cycles in dissipatively coupled condensates, Phys. Rev. B **101**, 085302 (2020).

[5] R. Hamerly and H. Mabuchi, Optical devices based on limit cycles and amplification in semiconductor optical cavities, Phys. Rev. Appl. **4**, 024016 (2015).

[6] P. Piergentili, W. Li, R. Natali, D. Vitali, and G. Di Giuseppe, Absolute determination of the single-photon optomechanical coupling rate via a Hopf bifurcation, Phys. Rev. Appl. **15**, 034012 (2021).

[7] R. M. May, Limit cycles in predator-prey communities, Science **177**, 900 (1972).

[8] M. E. Jewett and R. E. Kronauer, Refinement of limit cycle oscillator model of the effects of light on the human circadian pacemaker, J. Theor. Biol. **192**, 455 (1998).

[9] P. Turchin, *Complex Population Dynamics: A Theoretical/Empirical Synthesis (MPB-35)* (Princeton University Press, Princeton, New Jersey, 2003).

[10] R. Erban and H.-W. Kang, Chemical systems with limit cycles, Bull. Math. Biol. **85**, 76 (2023).

[11] M. Häusser, The Hodgkin-Huxley theory of the action potential, Nat. Neurosci. **3**, 1165 (2000).

[12] V. P. Golubyatnikov, I. V. Golubyatnikov, and V. A. Likhoshvai, On the existence and stability of cycles in five-dimensional models of gene networks, Numer. Analys. Appl. **3**, 329 (2010).

[13] A. Isidori, *Nonlinear Control Systems II, Communications and Control Engineering* (Springer-Verlag, New York, 2013).

[14] D. Witthaut, F. Hellmann, J. Kurths, S. Kettemann, H. Meyer-Ortmanns, and M. Timme, Collective nonlinear dynamics

and self-organization in decentralized power grids, Rev. Mod. Phys. **94**, 015005 (2022).
[15] D. Chalkiadakis and J. Hizanidis, Dynamical properties of neuromorphic Josephson junctions, Phys. Rev. E **106**, 044206 (2022).
[16] K. Seibold, R. Rota, and V. Savona, A dissipative time crystal in an asymmetric non-linear photonic dimer, Phys. Rev. A **101**, 033839 (2019).
[17] N. Carlon Zambon, S. R. Rodriguez, A. Lemaître, A. Harouri, L. Le Gratiet, I. Sagnes, P. St-Jean, S. Ravets, A. Amo, and J. Bloch, Parametric instability in coupled nonlinear microcavities, Phys. Rev. A **102**, 023526 (2020).
[18] M. Marconi, F. Raineri, A. Levenson, A. M. Yacomotti, J. Javaloyes, S. H. Pan, A. E. Amili, and Y. Fainman, Mesoscopic limit cycles in coupled nanolasers, Phys. Rev. Lett. **124**, 213602 (2020).
[19] J. Keeling, M. J. Bhaseen, and B. D. Simons, Collective dynamics of Bose-Einstein condensates in optical cavities, Phys. Rev. Lett. **105**, 043001 (2010).
[20] M. J. Bhaseen, J. Mayoh, B. D. Simons, and J. Keeling, Dynamics of nonequilibrium Dicke models, Phys. Rev. A **85**, 013817 (2011).
[21] T. E. Lee and H. R. Sadeghpour, Quantum synchronization of quantum van der Pol oscillators with trapped ions, Phys. Rev. Lett. **111**, 234101 (2013).
[22] F. Piazza and H. Ritsch, Self-organised limit-cycles, chaos and phase-slippage with a superfluid inside an optical resonator, Phys. Rev. Lett. **115**, 163601 (2015).
[23] E. I. R. Chiacchio and A. Nunnenkamp, Dissipation-induced instabilities of a spinor Bose-Einstein condensate inside an optical cavity, Phys. Rev. Lett. **122**, 193605 (2019).
[24] H. Keßler, J. G. Cosme, M. Hemmerling, L. Mathey, and A. Hemmerich, Emergent limit cycles and time crystal dynamics in an atom-cavity system, Phys. Rev. A **99**, 053605 (2019).
[25] K. J. H. Peters and S. R. K. Rodriguez, Limit cycles and chaos induced by a nonlinearity with memory, Eur. Phys. J.: Spec. Top. **231**, 247 (2022).
[26] P. Kongkhambut, J. Skulte, L. Mathey, J. G. Cosme, A. Hemmerich, and H. Keßler, Observation of a continuous time crystal, Science **377**, 670 (2022).
[27] L. Bello, M. C. Strinati, E. G. D. Torre, and A. Pe'er, Persistent coherent beating in coupled parametric oscillators, Phys. Rev. Lett. **123**, 083901 (2019).
[28] M. C. Strinati, I. Aharonovich, S. Ben-Ami, E. G. D. Torre, L. Bello, and A. Pe'er, Coherent dynamics in frustrated coupled parametric oscillators, New J. Phys. **22**, 085005 (2020).
[29] T. Inagaki, K. Inaba, T. Leleu, T. Honjo, T. Ikuta, K. Enbutsu, T. Umeki, R. Kasahara, K. Aihara, and H. Takesue, Collective and synchronous dynamics of photonic spiking neurons, Nat. Commun. **12**, 2325 (2021).
[30] A. Eichler and O. Zilberberg, *Classical and Quantum Parametric Phenomena* (Oxford University Press, Oxford, UK, 2023).
[31] C. Chen, D. H. Zanette, J. R. Guest, D. A. Czaplewski, and D. López, Self-sustained micromechanical oscillator with linear feedback, Phys. Rev. Lett. **117**, 017203 (2016).
[32] S. Houri, D. Hatanaka, M. Asano, R. Ohta, and H. Yamaguchi, Limit cycles and bifurcations in a nonlinear MEMS resonator with a 1:3 internal resonance, Appl. Phys. Lett. **114**, 103103 (2019).
[33] S. Houri, M. Asano, H. Okamoto, and H. Yamaguchi, Self-sustained libration regime in nonlinear microelectromechanical devices, Phys. Rev. Appl. **16**, 064015 (2021).
[34] W. Brenig, Spinless fermions in a Z_2 gauge theory on a triangular ladder, Phys. Rev. B **105**, 245105 (2022).
[35] S. Khan and H. E. Türeci, Frequency combs in a lumped-element Josephson-junction circuit, Phys. Rev. Lett. **120**, 153601 (2018).
[36] C. Metzger, M. Ludwig, C. Neuenhahn, A. Ortlieb, I. Favero, K. Karrai, and F. Marquardt, Self-induced oscillations in an optomechanical system driven by bolometric backaction, Phys. Rev. Lett. **101**, 133903 (2008).
[37] N. Lörch, J. Qian, A. Clerk, F. Marquardt, and K. Hammerer, Laser theory for optomechanics: Limit cycles in the quantum regime, Phys. Rev. X **4**, 011015 (2013).
[38] L. Bakemeier, A. Alvermann, and H. Fehske, Route to chaos in optomechanics, Phys. Rev. Lett. **114**, 013601 (2015).
[39] D. Navarro-Urrios, N. E. Capuj, M. F. Colombano, P. D. García, M. Sledzinska, F. Alzina, A. Griol, A. Martínez, and C. M. Sotomayor-Torres, Nonlinear dynamics and chaos in an optomechanical beam, Nat. Commun. **8**, 14965 (2017).
[40] T. F. Roque, F. Marquardt, and O. M. Yevtushenko, Nonlinear dynamics of weakly dissipative optomechanical systems, Nat. Rev. Phys. **2**, 229 (2019).
[41] J. Li, Z.-H. Zhou, S. Wan, Y.-L. Zhang, Z. Shen, M. Li, C.-L. Zou, G.-C. Guo, and C.-H. Dong, All-optical synchronization of remote optomechanical systems, Phys. Rev. Lett. **129**, 063605 (2022).
[42] Y. Ye and S.-l. Cai, *Theory of Limit Cycles* (American Mathematical Society, Providence, Rhode Island, 1986), Vol. 66.
[43] A. Jenkins, Self-oscillation, Phys. Rep. **525**, 167 (2013).
[44] A. Pikovsky, M. Rosenblum, and J. Kurths, *Synchronization - A Universal Concept in Nonlinear Sciences*, Cambridge Nonlinear Science Series, Vol. 12 (Cambridge University Press, Cambridge, UK, 2001), pp. 1–411.
[45] J. P. Thomas, E. H. Dowell, and K. C. Hall, Modeling viscous transonic limit cycle oscillation behavior using a harmonic balance approach, J. Aircr. **41**, 1266 (2004).
[46] E. P. Petrov, Analysis of flutter-induced limit cycle oscillations in gas-turbine structures with friction, gap, and other nonlinear contact interfaces, J. Turbomach. **134**, 061018 (2012).
[47] T. S. Parker and L. Chua, *Practical Numerical Algorithms for Chaotic Systems* (Springer-Verlag, New York, 2012).
[48] A. R. Champneys, Y. A. Kuznetsov, and B. Sandstede, A numerical toolbox for homoclinic bifurcation analysis, International Journal of Bifurcation and Chaos **06**, 867 (1996).
[49] R. Veltz, BifurcationKit.jl, https://hal.archives-ouvertes.fr/hal-02902346 (2020).
[50] G. Somieski, An eigenvalue method for calculation of stability and limit cycles in nonlinear systems, Nonlinear Dynamics **26**, 3 (2001).
[51] D. Davidenko, On the approximate solution of systems of nonlinear equations, Ukr. Mat. Zh **5**, 196 (1953).
[52] M. N. Jacovlev, On the solution of systems of nonlinear equations by differentiation with respect to a parameter, USSR Computational Math. and Math. Phys **4**, 146 (1964).
[53] G. H. Meyer, On solving nonlinear equations with a one-parameter operator imbedding, SIAM J. Numer. Anal. **5**, 739 (1968).

[54] W. Govaerts, Y. A. Kuznetsov, and A. Dhooge, Numerical continuation of bifurcations of limit cycles in MATLAB, SIAM J. Sci. Comput. **27**, 231 (2005).

[55] M. Han, Bifurcation theory of limit cycles of planar systems, in *Handbook of Differential Equations: Ordinary Differential Equations* (Elsevier, Amsterdam, Netherlands, 2006), Vol. 3, pp. 341–433.

[56] J. Guckenheimer and P. Holmes, *Nonlinear Oscillations, Dynamical Systems, and Bifurcations of Vector Fields*, Applied Mathematical Sciences (Springer-Verlag, New York, 1983), Vol. 42.

[57] D. Hilbert, Mathematische probleme, Nachrichten von der Koniglichen Gesellschaft der Wissenschaften zu Gottingen, 1900.

[58] R. Genesio and A. Tesi, Harmonic balance methods for the analysis of chaotic dynamics in nonlinear systems, Automatica **28**, 531 (1992).

[59] M. Guskov, J.-J. Sinou, and F. Thouverez, Multi-dimensional harmonic balance applied to rotor dynamics, Mech. Res. Commun. **35**, 537 (2008).

[60] A. C. Luo and J. Huang, Approximate solutions of periodic motions in nonlinear systems via a generalized harmonic balance, J. Vib. Control **18**, 1661 (2012).

[61] M. Krack and J. Gross, *Harmonic Balance for Nonlinear Vibration Problems* (Springer, Cham, Switzerland, 2019), p. 159.

[62] J. Košata, J. del Pino, T. L. Heugel, and O. Zilberberg, HarmonicBalance.jl: A Julia suite for nonlinear dynamics using harmonic balance, SciPost Phys. Codebases, 6 (2022).

[63] P. Breiding, M. Michałek, L. Monin, and S. Telen, The algebraic degree of coupled oscillators, arXiv:2208.08179.

[64] V. Borovik, P. Breiding, J. del Pino, M. Michałek, and O. Zilberberg, Khovanskii bases for semimixed systems of polynomial equations–approximating stationary nonlinear Newtonian dynamics, Journal de Mathématiques Pures et Appliquées **182**, 195 (2024).

[65] N. N. Bogoliubov and Y. A. Mitropolsky, *Asymptotic Methods in the Theory of Non-linear Oscillations* (Gordon and Breach, New York, 1961), Vol. 1.

[66] R. H. Rand, Lecture notes on nonlinear vibrations, http://audiophile.tam.cornell.edu/randdocs/nlvibe52.pdf (2005).

[67] A. J. Sommese and C. W. Wampler, *The Numerical Solution of Polynomial Systems Arising in Engineering and Science* (World Scientific, Singapore, 2005), pp. 1–402.

[68] P. Breiding and S. Timme, HomotopyContinuation.jl: A package for homotopy continuation in Julia, in *Lect. Notes Comput. Sci. (including Subser. Lect. Notes Artif. Intell. Lect. Notes Bioinformatics)*, Vol. 10931 LNCS (Springer, Cham, Switzerland, 2018), pp. 458–465.

[69] S. Timme, Numerical Nonlinear Algebra, Ph.D. thesis, Technische Universität Berlin, Germany, 2021.

[70] A. Leuch, L. Papariello, O. Zilberberg, C. L. Degen, R. Chitra, and A. Eichler, Parametric symmetry breaking in a nonlinear resonator, Phys. Rev. Lett. **117**, 214101 (2016).

[71] T. L. Heugel, O. Zilberberg, C. Marty, R. Chitra, and A. Eichler, Ising machines with strong bilinear coupling, Phys. Rev. Res. **4**, 013149 (2022).

[72] A. Bachtold, J. Moser, and M. I. Dykman, Mesoscopic physics of nanomechanical systems, Rev. Mod. Phys. **94**, 045005 (2022).

[73] L. A. Lugiato, *Ii Theory of Optical Bistability* (Elsevier, Amsterdam, Netherlands, 1984), pp. 69–216.

[74] R. Burgwal, J. del Pino, and E. Verhagen, Comparing nonlinear optomechanical coupling in membrane-in-the-middle and single-cavity systems, New J. Phys. **22**, 113006 (2020).

[75] D. A. Visani, L. Catalini, C. L. Degen, A. Eichler, and J. del Pino, Near-resonant nuclear spin detection with high-frequency mechanical resonators, arXiv:2311.16273.

[76] H. Alaeian, G. Giedke, I. Carusotto, R. Löw, and T. Pfau, Limit cycle phase and Goldstone mode in driven dissipative systems, Phys. Rev. A **103**, 013712 (2021).

[77] E. I. R. Chiacchio, A. Nunnenkamp, and M. Brunelli, Non-reciprocal Dicke model, Phys. Rev. Lett. **131**, 113602 (2023).

[78] D. Dreon, A. Baumgärtner, X. Li, S. Hertlein, T. Esslinger, and T. Donner, Self-oscillating pump in a topological dissipative atom–cavity system, Nature (London) **608**, 494 (2022).

[79] F. M. Fernández, Exceptional point in a simple textbook example, Eur. J. Phys. **39**, 045005 (2018).

[80] A. Khedri, D. Horn, and O. Zilberberg, Fate of exceptional points in the presence of nonlinearities, arXiv:2208.11205.

[81] E. J. Doedel, Auto: A program for the automatic bifurcation analysis of autonomous systems, Congr. Numer. **30**, 265 (1981).

[82] B. Ermentrout, XPPAUT 5.0-the Differential Equations Tool, University of Pittsburgh, Pittsburgh, 2001.

[83] B. Ermentrout and A. Mahajan, Simulating, analyzing, and animating dynamical systems: A guide to XPPAUT for researchers and students, Appl. Mech. Rev. **56**, B53 (2003).

[84] A. Dhooge, W. Govaerts, and Y. A. Kuznetsov, MATCONT: A MATLAB package for numerical bifurcation analysis of ODEs, ACM Trans. Math. Softw. **29**, 141 (2003).

[85] F. Schilder, H. Dankowicz, and M. Li, Continuation Core and Toolboxes (COCO), https://sourceforge.net/projects/cocotools, accessed: 2024-01-02.

[86] J. Košata, Spatial and temporal mode engineering in nonlinear media, ETH Zurich, 2022, doi:10.3929/ethz-b-000589190.

[87] L. D. Landau, On the problem of turbulence, Dokl. Akad. Nauk SSSR **44**, 339 (1944).

[88] J. T. Stuart, On the non-linear mechanics of hydrodynamic stability, J. Fluid Mech. **4**, 1 (1958).

[89] K. C. Hall, J. P. Thomas, and W. S. Clark, Computation of unsteady nonlinear flows in cascades using a harmonic balance technique, AIAA J. **40**, 879 (2002).

[90] A. Liénard, Etude des oscillations entretenues, Revue Generale de l'Elactricite **23**, 901 (1928).

[91] N. V. Kuznetsov, O. A. Kuznetsova, and G. A. Leonov, Visualization of four normal size limit cycles in two-dimensional polynomial quadratic system, Differ. Equ. Dyn. Syst. **21**, 29 (2013).

[92] Y. Yan, X. Dong, L. Huang, K. Moskovtsev, and H. B. Chan, Energy transfer into period-tripled states in coupled electromechanical modes at internal resonance, Phys. Rev. X **12**, 031003 (2022).

[93] S. Aldana, C. Bruder, and A. Nunnenkamp, Equivalence between an optomechanical system and a Kerr medium, Phys. Rev. A **88**, 043826 (2013).

[94] R. Chitra and O. Zilberberg, Dynamical many-body phases of the parametrically driven, dissipative Dicke model, Phys. Rev. A **92**, 023815 (2015).

[95] F. Ferri, R. Rosa-Medina, F. Finger, N. Dogra, M. Soriente, O. Zilberberg, T. Donner, and T. Esslinger, Emerging dissipative phases in a superradiant quantum gas with tunable decay, Phys. Rev. X **11**, 041046 (2021).

[96] A. Tusnin, A. Tikan, K. Komagata, and T. J. Kippenberg, Nonlinear dynamics and Kerr frequency comb formation in lattices of coupled microresonators, Commun. Phys. **6**, 317 (2023).

[97] C. W. Wächtler and G. Platero, Topological synchronization of quantum van der Pol oscillators, Phys. Rev. Res. **5**, 023021 (2023).

[98] J. N. Moreno, C. W. Wächtler, and A. Eisfeld, Synchronized states in a ring of dissipatively coupled harmonic oscillators, Phys. Rev. E **109**, 014308 (2024).

[99] S. Walter, A. Nunnenkamp, and C. Bruder, Quantum synchronization of a driven self-sustained oscillator, Phys. Rev. Lett. **112**, 094102 (2014).

[100] S. Walter, A. Nunnenkamp, and C. Bruder, Quantum synchronization of two Van der Pol oscillators, Annalen der Physik **527**, 131 (2015).

[101] M. Xu, D. A. Tieri, E. C. Fine, J. K. Thompson, and M. J. Holland, Synchronization of two ensembles of atoms, Phys. Rev. Lett. **113**, 154101 (2014).

[102] A. Roulet and C. Bruder, Quantum synchronization and entanglement generation, Phys. Rev. Lett. **121**, 063601 (2018).

[103] S. Sonar, M. Hajdušek, M. Mukherjee, R. Fazio, V. Vedral, S. Vinjanampathy, and L.-C. Kwek, Squeezing enhances quantum synchronization, Phys. Rev. Lett. **120**, 163601 (2018).

[104] A. Roulet and C. Bruder, Synchronizing the smallest possible system, Phys. Rev. Lett. **121**, 053601 (2018).

[105] A. Grimm, N. E. Frattini, S. Puri, S. O. Mundhada, S. Touzard, M. Mirrahimi, S. M. Girvin, S. Shankar, and M. H. Devoret, Stabilization and operation of a Kerr-cat qubit, Nature (London) **584**, 205 (2020).

[106] L. B. Arosh, M. C. Cross, and R. Lifshitz, Quantum limit-cycles and the Rayleigh and van der Pol oscillators, Phys. Rev. Res. **3**, 013130 (2021).

[107] V. Liška, T. Zemánková, P. Jákl, M. Šiler, S. H. Simpson, P. Zemánek, and O. Brzobohatý, PT-like phase transition and limit cycle oscillations in non-reciprocally coupled optomechanical oscillators levitated in vacuum, Nat. Phys. (2024), doi:10.1038/s41567-024-02590-1.

[108] M. Reisenbauer, H. Rudolph, L. Egyed, K. Hornberger, A. V. Zasedatelev, M. Abuzarli, B. A. Stickler, and U. Delić, Non-Hermitian dynamics and non-reciprocity of optically coupled nanoparticles, Nat. Phys. (2024), doi:10.1038/s41567-024-02589-8.

[109] D. Cox, J. Little, and D. O'Shea, *Ideals, Varieties, and Algorithms: An Introduction to Computational Algebraic Geometry and Commutative Algebra* (Springer, New York, NY, 2013).

[110] K. Lust and D. Roose, Computation and bifurcation analysis of periodic solutions of large-scale systems, in *Numerical Methods for Bifurcation Problems and Large-Scale Dynamical Systems*, edited by E. Doedel and L. S. Tuckerman (Springer New York, New York, NY, 2000), pp. 265–301.

[111] J. S. Umbría and M. Net, Numerical continuation methods for large-scale dissipative dynamical systems, Eur. Phys. J.: Spec. Top. **225**, 2465 (2016).

[112] J. Sánchez, M. Net, B. García-Archilla, and C. Simó, Newton-Krylov continuation of periodic orbits for Navier Stokes flows, J. Comput. Phys. **201**, 13 (2004).

[113] R. H. Clewley, W. E. Sherwood, M. D. LaMar, and J. M. Guckenheimer, Pydstool, a software environment for dynamical systems modeling (2007), http://pydstool.sourceforge.net.

[114] HarmonicBalance.jl documentation, https://nonlinearoscillations.github.io/HarmonicBalance.jl.